Published in final edited form as:
Adv Cancer Res. 2014 ; 124: 235–256. doi:10.1016/B978-0-12-411638-2.00007-0.

Molecular Imaging of the Tumor Microenvironment for Precision Medicine and Theranostics

Marie-France Penet[*,†], **Balaji Krishnamachary**[*], **Zhihang Chen**[*], **Jiefu Jin**[*], and **Zaver M. Bhujwalla**[*,†,1]

[*]JHU ICMIC Program, Division of Cancer Imaging Research, The Russell H. Morgan Department of Radiology and Radiological Science, The Johns Hopkins University School of Medicine, Baltimore, Maryland, USA

[†]Sidney Kimmel Comprehensive Cancer Center, The Johns Hopkins University School of Medicine, Baltimore, Maryland, USA

Abstract

Morbidity and mortality from cancer and their associated conditions and treatments continue to extract a heavy social and economic global burden despite the transformative advances in science and technology in the twenty-first century. In fact, cancer incidence and mortality are expected to reach pandemic proportions by 2025, and costs of managing cancer will escalate to trillions of dollars. The inability to establish effective cancer treatments arises from the complexity of conditions that exist within tumors, the plasticity and adaptability of cancer cells coupled with their ability to escape immune surveillance, and the co-opted stromal cells and microenvironment that assist cancer cells in survival. Stromal cells, although destroyed together with cancer cells, have an ever-replenishing source that can assist in resurrecting tumors from any residual cancer cells that may survive treatment. The tumor microenvironment landscape is a continually changing landscape, with spatial and temporal heterogeneities that impact and influence cancer treatment outcome. Importantly, the changing landscape of the tumor microenvironment can be exploited for precision medicine and theranostics. Molecular and functional imaging can play important roles in shaping and selecting treatments to match this landscape. Our purpose in this review is to examine the roles of molecular and functional imaging, within the context of the tumor microenvironment, and the feasibility of their applications for precision medicine and theranostics in humans.

1. INTRODUCTION

Cancer is a disease of cell survival. Unlike stroke or cardiac ischemia where the death of cells results in loss of organ function, cancer arises from cells uniquely adapted to survive damage. As a result, our current paradigms of treating cancer inflict significant collateral damage to normal tissues. Precision or personalized medicine (PM) is being strongly advocated as a solution to selectively targeting cancer cells and minimizing damage to normal tissue. The field of theranostics is creating exciting new possibilities for combining

[1]Corresponding author: zaver@mri.jhu.edu.

diagnosis with therapy in PM. Currently, most molecular-targeted treatments focus on genomic characterization of cancer cells but not on the microenvironment around tumors. Furthermore, unlike noninvasive imaging, biopsied tumor specimens do not provide a comprehensive characterization of the cancer.

Advances in molecular and functional imaging are providing new means to image intact cells and tumors and understand the interplay between cancer cells and the microenvironment that surrounds these cells. These advances can find important niches in PM and theranostics of the tumor microenvironment (TME) (Fig. 7.1). The networks of blood and lymphatic vessels, stromal cells, and the extracellular matrix (ECM) that are collectively termed the TME are co-opted and shaped by cancer cells to survive, invade, and form distant metastasis. Abnormalities in vasculature, lymphatics, and metabolism impose additional heterogeneities in hypoxia, interstitial pressure, and acidic microenvironments. These factors can provide transcriptional signals that alter gene and protein expression. The TME therefore presents an ever-changing landscape of spatial and temporal heterogeneities in physiology, metabolism, and stromal cell trafficking, highlighting the importance of using noninvasive imaging to follow these dynamics. Many of the lethal consequences of these changing landscapes, such as hypoxia, result in a cascade of changes in multiple pathways and networks and have lethal repercussions such as recurrence and metastasis that become evident only several years later.

Stromal cells such as cancer-associated fibroblasts (CAFs) and tumor-associated macrophages (TAMs) mediate many of the aggressive characteristics of cancer but have an ever-replenishing supply left largely intact by our current therapeutic strategies. Therefore, even following surgery or radiation or chemotherapy, a few cancer cells that ordinarily would not survive on their own continue to have a host of stromal cells to assist them in reestablishment at local or distant sites. In this review, we have focused on highlighting the most recent advances in molecular and functional imaging and nanoparticles that incorporate, or have the potential to be incorporated in, molecular and functional imaging of the TME for PM and theranostics in cancer. The resurgence of interest in delivering molecular reagents such as complementary DNA (cDNA), small interfering RNA (siRNA), and microRNA provides new opportunities for image-guided delivery of nanoparticles carrying these agents. Theranostic agents targeting cancer cells that combine imaging probes with siRNA have been developed, and their efficacy in target delivery and message downregulation has been demonstrated (Chen et al., 2012; Li et al., 2010; Medarova, Pham, Farrar, Petkova, & Moore, 2007).

2. IMAGING AND PM/THERANOSTICS OF THE PHYSIOLOGICAL MICROENVIRONMENT

2.1. Hypoxia

Poor oxygenation, arising from the chaotic and abnormal tumor vasculature, has been identified as a major cause of radiation resistance since the 1950s when Thomlinson and Gray detected necrosis occurring in human lung cancers at a distance of 150 μm from the nearest blood vessels (Thomlinson & Gray, 1955). The oxygen effect, where increased

formation of free radicals results in increased radiation damage in the presence of oxygen and decreased radiation damage in the absence of oxygen was established by then (Gray, Conger, Ebert, Hornsey, & Scott, 1953), allowing Thomlinson and Gray to make the prescient observation that hypoxia must exist in human tumors and cause radiation resistance. With the discovery of the hypoxia-inducible factors (HIFs) and hypoxia response elements (HREs) that transcriptionally regulate several genes, the past decade has witnessed an every-burgeoning interest in the role of hypoxia and evidence of the role of HIFs in cancer progression, invasion, metastasis, and resistance to treatment (Semenza, 2010). In addition, the constitutive stabilization of HIF in cancers such as renal cell carcinoma has led to the development of HIF inhibitors in cancer treatment (Onnis, Rapisarda, & Melillo, 2009).

Several imaging modalities can be applied to image tumor hypoxia. PET imaging probes of hypoxia such as ^{18}F-fluoromisonidazole [^{18}F-FMISO], ^{18}F-flortanidazole [^{18}F-HX4], ^{18}F-fluoroazomycin arabinoside [^{18}F-FAZA], and ^{64}Cu-diacetyl-*bis*(N_4-methylsemicarbazone) [^{64}Cu-ATSM] rely on their ability to bind to molecules in viable hypoxic cells allowing *in vivo* detection of hypoxia (Carlin et al., 2014; Spence et al., 2008). Clinical applications of such probes can be used to tailor intensity-modulated radiation therapy to hypoxia within tumors as shown in proof-of-principle studies (Servagi-Vernat et al., 2014). Clinical trials demonstrating improved patient survival are not available as yet but are necessary to provide further confirmation of the importance of using imaging for PM of hypoxia. FMISO PET was used to assess the hypoxic status of tumors in a study conducted on 22 patients with glioblastoma multiforme (GBM) (Fig. 7.2). A greater volume of hypoxic regions and the maximum intensity of the probe before radiotherapy were strongly associated with poor survival (Spence et al., 2008).

Magnetic resonance spectroscopy (MRS) probes have also been developed to detect oxygenation based on the dependence of the relaxivity of hexamethyldisoloxane (HMDSO) (^{1}H MRS) and perfluorocarbons (^{19}F MRS) on oxygen tensions (Mason, Shukla, & Antich, 1993). HMDSO has been used to determine oxygen tension in an experimental model of prostate cancer with ^{1}H MRS after intravenous (i.v.) injection (Kodibagkar, Cui, Merritt, & Mason, 2006). The ^{19}F probe 2-nitro-α-[(2,2,2-trifluoroethoxy)methyl]-imidazole-1-ethanol is a nitroimidazole-based probe that is reduced in hypoxic cells and binds to endogenous cellular molecules. Its accumulation can be used to report on hypoxia *in vivo* with ^{19}F MRS (Procissi et al., 2007). Very few first-in-human studies have been performed so far (Lee et al., 2009). The nitroimidazole hypoxia marker SR4554 was tested in 26 patients in various malignancies, with a predominance of gastrointestinal stromal tumors, head and neck cancer, and melanoma. Tumors that were at least 3 cm in size and no more than 4 cm depth were investigated to allow acquisition of ^{19}F MRS data with a surface coil. While the study showed the feasibility of using MRS to study the retention of the probe in some tumors, it also highlighted the low sensitivity of MRS compared to PET (Lee et al., 2009).

A new nitroimidazole-based T_1 MR contrast agent, gadolinium tetraazacyclododecanetetraacetic acid monoamide conjugate of 2-nitro- imidazole ($GdDO_3NI$), was recently developed to image tumor hypoxia and was found to accumulate

significantly in the central poorly perfused regions of a rat prostate cancer xenograft (Gulaka et al., 2014).

Optical images probes, created from linking the HRE to fluorescent protein expression, have also been developed by creating cancer cell lines expressing this construct (Raman et al., 2006). These have been exclusively used in xenograft models for basic research to understand the relationship between vasculature and hypoxia (as shown in Fig. 7.3) and the effect of hypoxia on collagen 1 fiber distribution, metabolism, and macromolecular transport (Kakkad et al., 2010, 2013; Raman et al., 2006). While these reporters are useful for basic research, their applications for PM in humans are not feasible and they are primarily valuable research tools.

Some advances have been made in creating HRE-driven therapeutic genes such as cytosine deaminase in targeting hypoxia as these will only be expressed in hypoxic regions (Marignol et al., 2009). Although these are only at the basic research stage, they show promise for PM of hypoxia in the future, especially with recent advances in nanoparticle-based delivery of molecular reagents such as siRNA and cDNA.

2.2. pH

The acidic extracellular pH (pH_e) that exists within cancers because of poor perfusion and increased glycolytic activity is another environmental factor that can influence progression and treatment outcome (Gillies & Gatenby, 2007; Gillies, Robey, & Gatenby, 2008). ^{31}P MRS can detect intracellular pH (pH_i) from the chemical shift of the inorganic phosphate signal, or pH_e from the chemical shift of an exogenous ^{31}P-detectable pH marker such as 3-aminopropylphosphonate (Robey et al., 2009). The low sensitivity of ^{31}P MRS, however, results in limited spatial resolution. To improve spatial resolution, pH_e imaging has been performed in tumors *in vivo* using probes detected with ^{1}H MRSI such as (imidazol-1-yl)3-ethyoxycarbonylpropionic acid (van Sluis et al., 1999), or 2-(imidazol-1-yl)succinic acid (Provent et al., 2007).

Optical probes have been also developed to image acidosis in tumors such as a pH-activated near infrared (NIR) fluorescent probe (Wang, Zhu, et al., 2012). Optical imaging with its high sensitivity and fast acquisition rate presents several advantages. With NIR fluorescence, autofluorescence and absorbance from endogenous molecules are low, improving the sensitivity and spatial resolution in deep tissues. One recently described probe, DiIR783-S, is activated at low pH by the cleavage of hydrazine bonds leading to a reduced self-quenching effect and to the activation of NIR fluorescence (Wang, Zhu, et al., 2012). The probe was successfully tested in an MDA-MB-435 xenograft model and allowed *in vivo* visualization of tumor acidosis (Fig. 7.4).

There are currently no pH imaging probes available for applications in humans. The most likely candidates in the future will be chemical exchange saturation transfer (CEST) pH probes (Chen et al., 2013) and hyperpolarized ^{13}C probes (Gallagher et al., 2008). pH_e imaging with CEST was recently demonstrated in a breast cancer xenograft model using a clinically approved CT contrast agent, iopromide (Chen et al., 2013). The ratio of the CEST effects of the two amide protons of iopromide linearly correlated with pH 6.3–7.2

independently of the concentration. Tissue pH was also determined *in vivo* following an i.v. injection of hyperpolarized $H^{13}CO_3^-$, by measuring the concentrations of $H^{13}CO_3^-$ and $^{13}CO_2$ formed and deriving pH from the Henderson–Hasselbalch equation ($pH = pK_a + \log_{10}([HCO_3^-]/[CO_2])$; Gallagher et al., 2008). The technique was successfully applied *in vivo* to measure pH in a preclinical model of lymphoma (Gallagher et al., 2008).

In addition to characterizing the aggressiveness of cancers with pH imaging, PM incorporating pH imaging can utilize the use of pH-sensitive carriers to specifically deliver drugs to the acidic TMEs. Polymeric micelles displaying pH sensitivity and controlled release have been designed to carry and deliver hydrophobic agents to tumors (Gao, Li, & Lee, 2013). These pH-sensitive polymers consist of ionizable groups that can accept or donate protons in response to environmental pH changes (Gao et al., 2013). At physiological pH, polymeric micelles self-assemble from amphiphilic block copolymers. Water-insoluble imaging agents or drugs can then be encapsulated into the micelles *via* hydrophobic interactions. These micelles can be ionized and solubilized in the low pH_e of the TME and subsequently be used for cancer diagnostics and targeted therapies. Doxorubicin-loaded pH-responsive polymeric micelle with pH-dependent micellization–demicellization transitions have been recently developed (Ko et al., 2007). *In vitro* experiments revealed that these doxorubicin-loaded micelles prevented drug release at pH 7.4, while releasing more than 70% of the drug cargo over 6 h at pH 6.4. B16F10 melanoma tumor cell uptake of doxorubicin released from the micelles was much higher at pH 6.4 than at pH 7.4. The antitumor efficacy of the pH-responsive polymeric micelles was also tested *in vivo*. A suppression of B16F10 tumor growth and a prolonged survival of the treated tumor-bearing mice compared to control mice were observed (Ko et al., 2007).

3. THE ECM AND ITS ENZYMES

Proteases overexpressed by both cancer cells and stromal cells shape the ECM and can be exploited for imaging and therapeutic purposes. Protease activity can be used to activate imaging or therapeutic agents specifically in the tumor. Among the proteases, matrix metalloproteinases (MMPs) and cathepsin B play a critical role in tumor progression and metastases. MMPs, a family of 26 secreted and transmembrane proteins can degrade the ECM and regulate the activity of other proteases, receptors, and growth factors. Cathepsin B is a lysosomal cysteine protease that is overexpressed in several tumor types. It converts pro-urokinase-type plasminogen activator to urokinase-type plasminogen activator, activating plasminogen to plasmin, a serine protease, which can degrade several components of the ECM such as fibrin, fibronectin, laminin, and proteoglycans. Many activatable NIR probes that are based on fluorescence resonance energy transfer are available to detect protease activity. The targeting of these proteases have been successfully developed and widely explored in biomedical research (Weidle, Tiefenthaler, & Georges, 2014).

Along similar principles, several prodrug therapeutics have been developed that are specifically activated after cleavage by a protease. The different proteases used as mediators of cytotoxicity in tumor therapy were recently reviewed (Weidle et al., 2014) and highlight the diversity of recently developed therapeutic and imaging probes.

Excess remodeling of collagen fibers is commonly seen in tumors. During this remodeling, large portions of collagen are degraded and denatured by proteolytic enzymes. A probe that specifically binds to cryptic sites in collagen strands that become exposed when denatured was recently described and can be used for diagnostic and therapeutic purposes (Li, Foss, et al., 2012). Fluorescently labeled collagen mimetic peptides (CMP) were used *in vivo* to target and image denatured collagens in a prostate tumor xenograft (Fig. 7.5). The NIR fluorophore-labeled CMP probe (IR-Ahx-$(GPO)_9$) permeated through tumor vasculature and accumulated in the tumor while the scrambled control sequence (IR-Ahx-$^{S}G_9P_9O_9$) showed minimal accumulation (Fig. 7.5A). Colocalization of the probe with MMP activity was demonstrated after MMPSense680 injection (Fig. 7.5B).

Direct imaging of collagen 1 fibers in the ECM is also possible with second harmonic generation microscopy (Brown et al., 2003). These fibers have been implicated in facilitating metastatic dissemination (Kakkad et al., 2012; Provenzano et al., 2006). The availability of biopsy compatible miniaturized fiber optic probes to detect second harmonic signal from tumor tissue could assist in identifying aggressive cancers that are likely to metastasize and assist in PM of the ECM.

Characterizing the movement of macromolecules through the ECM provides a measure of its integrity. Because proteolytic enzymes degrade the ECM, indices of integrity or porosity can be used to characterize the invasiveness of tumors. MRI of the macromolecular contrast agent albumin–gadolinium–DTPA was used to characterize the extravascular transport of macromolecules through the ECM of solid tumors *in vivo* and detected significant differences in transport indices such as pooling and draining volumes and rates between noninvasive and invasive breast cancer xenografts (Pathak et al., 2013). Insights into differences in macromolecular transport in hypoxic and normoxic tumor regions were also obtained with this approach (Kakkad et al., 2013).

4. ENDOTHELIAL CELLS AND TUMOR VASCULATURE

The vasculature established by tumors is one of the most widely investigated aspects of the TME. The chaotic vasculature of tumors has long been identified as a major barrier in effective drug delivery (Fukumura & Jain, 2007). This chaotic vasculature also results in hypoxia, substrate depletion, and extracellular acidosis (Gillies, Raghunand, Karczmar, & Bhujwalla, 2002). It is also one of the means by which cancer cells escape on their metastatic journey (Quail & Joyce, 2013). Tumor angiogenesis, the mechanism by which cancer cells establish vascularization, has been extensively investigated using MRI (Pathak, Penet, & Bhujwalla, 2010), PET, CT (Iagaru & Gambhir, 2013), and optical imaging (Eisenblatter, Holtke, Persigehl, & Bremer, 2010). More recently, angiogenesis has been visualized with molecular photoacoustic imaging (Pan et al., 2011). Photoacoustic tomography combines optical absorption contrast and fine ultrasonic resolution to generate high-resolution images of microvasculature using the inherent signal of hemoglobin that can be translated for human applications. To differentiate neovasculature from maturing microvasculature, $\alpha_v\beta_3$-gold nanobeacons have been developed and provided a sensitive and specific discrimination and quantification of angiogenesis *in vivo* as shown in a mouse Matrigel-plug model (Pan et al., 2011).

Integrins, such as $\alpha_5\beta_1$ and $\alpha_v\beta_3$, are poorly expressed on normal quiescent vessels, but are highly expressed on tumor blood vessels, and they can be used as specific targets for imaging and therapeutics. Changes in tumor neo-vasculature can be followed over time, as shown in Fig. 7.6, using gadolinium–DTPA–PE nanoparticles (Schmieder et al., 2013) that target $\alpha_v\beta_3$ integrins, allowing a longitudinal monitoring of tumor progression with the exploration of temporal–spatial patterns of angiogenesis in individual animals. A therapeutic component can be added to $\alpha_v\beta_3$-targeted nanoparticles (gadolinium–DTPA–BOA) by loading them with anti-angiogenic agents, such as fumagillin (Winter et al., 2008). Particle delivery can be further improved by targeting $\alpha_5\beta_1$ and $\alpha_v\beta_3$ integrins simultaneously, as demonstrated in an MDA-MB-435 breast cancer xenograft model. The efficacy of the fumagillin treatment on the angiogenesis was also improved as demonstrated using 3D MRI (Schmieder et al., 2008).

Tumor vascular targeting has been performed using other nanocarriers, such as liposomes, labeled with MR contrast agent and loaded with anticancer drugs, such as doxorubicin (Grange et al., 2010) or prednisolone phosphate (Cittadino et al., 2012). To increase the specificity of delivery, liposomes can be functionalized with specific ligands, such as peptides or antibodies to bind to molecules that are expressed on the cancer cell or the endothelial cell surface. The presence of MR contrast agent allows imaging of the delivery with MRI. Neural cell adhesion molecule (NCAM) is expressed by Kaposi's cells and tumor endothelial cells and can be targeted by a peptide. Liposomes carrying gadolinium and doxorubicin were developed to target NCAM in a Kaposi sarcoma model. The treatment resulted in reduced tumor growth and an increase of survival (Grange et al., 2010).

Magnetic targeting is another strategy that can be applied to improve nanoparticle delivery, as shown in a mouse subcutaneous xenograft model, using magnetic nanoparticles that contain a single superparamagnetic iron oxide core (Fu et al., 2012). In this strategy, an external permanent magnet producing a moderate magnetic field was combined with a tissue-embedded magnetizable micromesh that produced strong localized magnetic field gradients to attract individual magnetic nanoparticles to multiple locations of the mesh (Fu et al., 2012). In a human glioblastoma mouse model, the nanoparticles were magnetically retained in the tumor neovasculature and in the surrounding tumor tissues, as observed by fluorescence intravital microscopy in real time. The retention of the particles was improved by combining $\alpha_v\beta_3$ integrin targeting with magnetic targeting in a human glioblastoma mouse xenograft model. Tumor regression occurred more rapidly using combined targeting as compared to the integrin targeting alone (Fu et al., 2012).

Normalizing the TME to improve drug delivery and efficacy of molecular medicines has also been proposed as a strategy to improve treatment outcome (Jain, 2013). Normalization of the tumor vasculature, lymphatic vessels, and the ECM can be assessed noninvasively using MRI, and the imaging results can be used to establish the time window during which patients should be treated. Contrast-enhanced CT perfusion measurement was recently used to predict tumor drug response in GBM patients (Pascal et al., 2013). These studies demonstrated the importance of the fraction of blood volume, the distribution of tumor vessel diameter, and the distance that drugs diffuse through the tissue for effective drug delivery. These parameters differ between tumor types, and between individuals with a

similar tumor type, and should be assessed individually to design successive chemotherapy cycles based on the characteristics of the tumor vasculature (Pascal et al., 2013).

5. LYMPHATIC ENDOTHELIAL CELLS, LYMPHATICS, AND INTERSTITIAL PRESSURE

The lymphatic system is an important route of metastases, facilitating tumor dissemination from primary sites to distant tissues. Like the vasculature, lymphatics within tumors are chaotic and nonfunctional resulting in the build-up of interstitial fluid pressure that further contributes to poor transport of molecules through the ECM (Fukumura & Jain, 2007). While most imaging studies have focused on imaging lymph node metastases and nodal staging (Harisinghani et al., 2003; Ross et al., 2009; Seenu et al., 2005), some have explored ways to image lymphangiogenesis. Lymphatic endothelial cells (LECs) present specific antigens on their surface, such as LYVE-1, VEGFR3, and podoplanin. Podoplanin is a membrane mucin, which promotes endothelial cell adhesion, migration, and lymphatic formation (Yang et al., 2013), and can be targeted to image lymphangiogenesis noninvasively. GoldMag nanoparticle is a new superparamagnetic composite composed of an ultrasmall superparamagnetic iron oxide core and a colloidal gold shell. Water-soluble PEG-GoldMag nanoparticles bound to antipodoplanin antibodies were used to show the feasibility of imaging lymphangiogenesis with MRI in a breast cancer model (Yang et al., 2013). LyP-1 is a cyclic peptide that binds not only to some cancer cells but also to tumor lymphatic vessels (Wang, Yu, et al., 2012). Added to the surface of polymeric micelles loaded with artemisinin, the peptide improved the specificity of particle delivery to MDA-MB-435 tumors and LECs, as shown *in vivo* with NIR fluorescent imaging (Wang, Yu, et al., 2012). Artemisinin is a natural product with potential anticancer and antilymphangiogenesis effects. Targeted micelles loaded with artemisinin achieved a higher antitumor efficacy than nontargeted ones, demonstrating their potential as effective theranostic agents targeting metastatic breast cancer cells and lymphatics (Wang, Yu, et al., 2012).

6. STROMAL COMPONENTS OF THE TME AND THEIR ROLE IN PM

Stromal cells play a critical role in tumor progression (Quail & Joyce, 2013). Among them, CAFs significantly influence the proliferation, invasion, and metastasis of cancer cells. Fibroblast activation protein-α (FAPα) is a cell surface glycoprotein and a member of the serine protease family that has been found to be selectively produced by CAFs that can be used to image CAFs *in vivo*. FAPα-targeted imaging probes could be used for early detection of cancer, stratification of cancer patients for FAPα-targeted therapy, and monitoring treatment response. A new probe that consists of a NIR dye (Cy5.5) and a quencher dye (QSY21) which are linked together by a short peptide sequence (KGPGPNQC) specific for FAPα cleavage was recently developed to detect CAFs (Li, Chen, et al., 2012). NIR fluorescence signal was observed after cleavage of the peptide sequence by FAPα both *in vitro* and *in vivo*. *In vivo* imaging demonstrated that the probe was rapidly activated in FAPα-positive U87MG tumors but not in negative C6 tumors, providing a novel FAPα-specific probe to quantify the presence of CAFs (Li, Chen, et al., 2012).

MRI has frequently been used in preclinical models to image stromal cells in the TME. CAFs (Granot et al., 2007), stem cells (Chaumeil et al., 2012), endothelial precursor cells (Anderson et al., 2005), natural killer cells (Daldrup-Link et al., 2005), T cells (Hu, Kettunen, & Brindle, 2005), and TAMs (Daldrup-Link et al., 2011; Shih et al., 2011) were imaged *in vivo* after being labeled with either T_1 or T_2 contrast agents.

To optimize the development of stem-cell-based therapies for the treatment of glioblastoma, the tropism of micron-size particles of iron oxide (MPIO)-labeled stem cell was explored *in vivo* as shown in Fig. 7.7 (Chaumeil et al., 2012). Labeled cells injected in the contralateral hemisphere of U87vIII tumor-bearing mice exhibited tropism to tumors, first localizing at the tumor edges, then in the tumor masses. Areas of hypointensity arising from the accumulation of labeled stem cells, colocalized first with gadolinium enhanced regions (i.e., regions of high vascular permeability), consistent with stem cell tropism to vascular endothelial growth factor.

More recently, fibroblasts overexpressing ferritin heavy chain (FHC) were engineered and used to quantitatively monitor the dynamic perivascular recruitment in ovarian carcinoma xenografts (Vandsburger et al., 2013). FHC overexpression combined with R_2 mapping and MR relaxometry enabled *in vivo* imaging of the recruitment of exogenously administered fibroblasts to the vasculature of ovarian tumor xenografts (Vandsburger et al., 2013).

7. INTRAOPERATIVE OPTICAL IMAGING

One of the most important advances in PM is the development of specialized intraoperative imaging systems for open surgery using NIR fluorescence to visualize cancer cells and tumor margins to facilitate image-guided surgery. Clinical applications have been described in sentinel lymph nodes mapping, in tumor imaging, and in vascularization and perfusion tumor imaging (Vahrmeijer, Hutteman, van der Vorst, van de Velde, & Frangioni, 2013).

The ability to visualize minuscule tumor deposits is essential to ensure complete resection of the tumor. $\alpha_v\beta_3$ integrin-targeted NIR fluorescent probes have been developed for intraoperative imaging and tested in an ovarian cancer model (Harlaar et al., 2013). The study showed that the probes could assist the surgeon in finding small tumor spots to resect with a sensitivity of 100%, a specificity of 88%, and a diagnostic accuracy of 96.5%. Fluorescence epiillumination imaging was used to remove all suspicious fluorescent spots by image-guided surgery, and hematoxylin and eosin histopathology was used to confirm the presence of cancer cells in the samples resected (Harlaar et al., 2013). A similar study was performed in ovarian cancer patients using a fluorescent probe targeting the folate receptor-α for *in vivo* tumor-specific imaging (van Dam et al., 2011). Applying image-guided intraoperative technique should lead to more efficient cyto-reduction, especially in cancers with a peritoneal dissemination pattern. Tumor-specific detection strategy should ultimately improve patient survival by providing real-time feedback on residual malignant tissue to the surgeon (van Dam et al., 2011).

Another important strategy for intraoperative and superficial tumors PM is the use of photoimmunotherapy (PIT) using NIR-photosensitizing dyes (Mitsunaga et al., 2011). In this novel molecular-targeted cancer therapy, a target-specific photosensitizer based on an

NIR phthalocyanine dye, IR700, is conjugated to monoclonal antibodies targeting epidermal growth factor receptors. The dye can be detected with optical imaging. *In vitro* cell death was induced immediately after irradiating monoclonal antibody-IR700-bound target cells with NIR light. *In vivo* tumor shrinkage after irradiation with NIR light was also described in target cells expressing the epidermal growth factor receptor. The study demonstrates the potential of target-selective PIT for the treatment of cancer based on monoclonal antibody binding to the cancer cell membrane (Mitsunaga et al., 2011).

8. CONCLUDING REMARKS

Molecular and functional imaging is finding transformative applications in PM and theranostics of cancer. In combination with advances in molecular medicine and the delivery of molecular reagents such as siRNA and cDNA, the exciting strategies being developed to visualize and target nearly every aspect of the TME and their rapid clinical translation should significantly advance our abilities to effectively treat and control a disease that currently continues to elude control and cure.

Acknowledgments

Support from NIH R01 CA136576, R01 CA138515, R01 CA73850, R01 CA82337, R01 CA154725, R01 CA134695, P50 CA103175, and P30 CA006973 is gratefully acknowledged.

ABBREVIATIONS

CAFs	cancer-associated fibroblasts
cDNA	complementary DNA
CEST	chemical exchange saturation transfer
CMP	collagen mimetic peptides
ECM	extracellular matrix
FAPα	fibroblast activation protein-α
^{18}F-FMISO	^{18}F-fluoromisonidazole
GBM	glioblastoma multiforme
HIFs	hypoxia-inducible factors
HREs	hypoxia response elements
LECs	lymphatic endothelial cells
MMPs	matrix metalloproteinases
MPIO	micron-size particles of iron oxide
NCAM	neural cell adhesion molecule
NIR	near infrared
pH_e	extracellular pH

pH_i	intracellular pH
PIT	photoimmunotherapy
PM	personalized medicine
siRNA	small interfering RNA
TAMs	tumor-associated macrophages
TME	tumor microenvironment

References

Anderson SA, Glod J, Arbab AS, Noel M, Ashari P, Fine HA, et al. Non-invasive MR imaging of magnetically labeled stem cells to directly identify neo-vasculature in a glioma model. Blood. 2005; 105(1):420–425. [PubMed: 15331444]

Brown E, McKee T, diTomaso E, Pluen A, Seed B, Boucher Y, et al. Dynamic imaging of collagen and its modulation in tumors in vivo using second-harmonic generation. Nature Medicine. 2003; 9(6):796–800.

Carlin S, Zhang H, Reese M, Ramos NN, Chen Q, Ricketts SA. A comparison of the imaging characteristics and microregional distribution of 4 hypoxia PET tracers. Journal of Nuclear Medicine: Official Publication, Society of Nuclear Medicine. 2014; 55(3):515–521.

Chaumeil MM, Gini B, Yang H, Iwanami A, Sukumar S, Ozawa T, et al. Longitudinal evaluation of MPIO-labeled stem cell biodistribution in glioblastoma using high resolution and contrast-enhanced MR imaging at 14.1 tesla. Neuro-Oncology. 2012; 14(8):1050–1061. [PubMed: 22670012]

Chen, LQ.; Howison, CM.; Jeffery, JJ.; Robey, IF.; Kuo, PH.; Pagel, MD. Evaluations of extracellular pH within in vivo tumors using acidoCEST MRI. Magnetic Resonance in Medicine: Official Journal of the Society of Magnetic Resonance in Medicine/Society of Magnetic Resonance in Medicine. 2013. http://dx.doi.org/10.1002/mrm.25053, [Epub ahead of print]

Chen Z, Penet MF, Nimmagadda S, Li C, Banerjee SR, Winnard PT Jr, et al. PSMA-targeted theranostic nanoplex for prostate cancer therapy. ACS Nano. 2012; 6(9):7752–7762. [PubMed: 22866897]

Cittadino E, Ferraretto M, Torres E, Maiocchi A, Crielaard BJ, Lammers T, et al. MRI evaluation of the antitumor activity of paramagnetic liposomes loaded with prednisolone phosphate. European Journal of Pharmaceutical Sciences: Official Journal of the European Federation for Pharmaceutical Sciences. 2012; 45(4):436–441. [PubMed: 21896328]

Daldrup-Link HE, Golovko D, Ruffell B, Denardo DG, Castaneda R, Ansari C, et al. MRI of tumor-associated macrophages with clinically applicable iron oxide nanoparticles. Clinical Cancer Research: An Official Journal of the American Association for Cancer Research. 2011; 17(17): 5695–5704. [PubMed: 21791632]

Daldrup-Link HE, Meier R, Rudelius M, Piontek G, Piert M, Metz S, et al. In vivo tracking of genetically engineered, anti-HER2/neu directed natural killer cells to HER2/neu positive mammary tumors with magnetic resonance imaging. European Radiology. 2005; 15(1):4–13. [PubMed: 15616814]

Eisenblatter M, Holtke C, Persigehl T, Bremer C. Optical techniques for the molecular imaging of angiogenesis. European Journal of Nuclear Medicine and Molecular Imaging. 2010; 37(Suppl 1):S127–S137. [PubMed: 20632173]

Fu A, Wilson RJ, Smith BR, Mullenix J, Earhart C, Akin D, et al. Fluorescent magnetic nanoparticles for magnetically enhanced cancer imaging and targeting in living subjects. ACS Nano. 2012; 6(8): 6862–6869. [PubMed: 22857784]

Fukumura D, Jain RK. Tumor microenvironment abnormalities: Causes, consequences, and strategies to normalize. Journal of Cellular Biochemistry. 2007; 101(4):937–949. [PubMed: 17171643]

Gallagher FA, Kettunen MI, Day SE, Hu DE, Ardenkjaer-Larsen JH, Zandt R, et al. Magnetic resonance imaging of pH in vivo using hyperpolarized 13C-labelled bicarbonate. Nature. 2008; 453(7197):940–943. [PubMed: 18509335]

Gao GH, Li Y, Lee DS. Environmental pH-sensitive polymeric micelles for cancer diagnosis and targeted therapy. Journal of Controlled Release: Official Journal of the Controlled Release Society. 2013; 169(3):180–184. [PubMed: 23195533]

Gillies RJ, Gatenby RA. Hypoxia and adaptive landscapes in the evolution of carcinogenesis. Cancer Metastasis Reviews. 2007; 26(2):311–317. [PubMed: 17404691]

Gillies RJ, Raghunand N, Karczmar GS, Bhujwalla ZM. MRI of the tumor microenvironment. Journal of Magnetic Resonance Imaging. 2002; 16(4):430–450. [PubMed: 12353258]

Gillies RJ, Robey I, Gatenby RA. Causes and consequences of increased glucose metabolism of cancers. Journal of Nuclear Medicine. 2008; 49(Suppl 2):24S–42S. [PubMed: 18523064]

Grange C, Geninatti-Crich S, Esposito G, Alberti D, Tei L, Bussolati B, et al. Combined delivery and magnetic resonance imaging of neural cell adhesion molecule-targeted doxorubicin-containing liposomes in experimentally induced Kaposi's sarcoma. Cancer Research. 2010; 70(6):2180–2190. [PubMed: 20215497]

Granot D, Addadi Y, Kalchenko V, Harmelin A, Kunz-Schughart LA, Neeman M. In vivo imaging of the systemic recruitment of fibroblasts to the angiogenic rim of ovarian carcinoma tumors. Cancer Research. 2007; 67(19):9180–9189. [PubMed: 17909023]

Gray LH, Conger AD, Ebert M, Hornsey S, Scott OC. The concentration of oxygen dissolved in tissues at the time of irradiation as a factor in radiotherapy. The British Journal of Radiology. 1953; 26(312):638–648. [PubMed: 13106296]

Gulaka PK, Rojas-Quijano F, Kovacs Z, Mason RP, Sherry AD, Kodibagkar VD. GdDO3NI, a nitroimidazole-based T1 MRI contrast agent for imaging tumor hypoxia in vivo. Journal of Biological Inorganic Chemistry: JBIC: A Publication of the Society of Biological Inorganic Chemistry. 2014; 19(2):271–279. [PubMed: 24281854]

Harisinghani MG, Barentsz J, Hahn PF, Deserno WM, Tabatabaei S, van de Kaa CH, et al. Noninvasive detection of clinically occult lymph-node metastases in prostate cancer. The New England Journal of Medicine. 2003; 348(25):2491–2499. [PubMed: 12815134]

Harlaar NJ, Kelder W, Sarantopoulos A, Bart J, Themelis G, van Dam GM, et al. Real-time near infrared fluorescence (NIRF) intra-operative imaging in ovarian cancer using an alpha(v)beta(3-)integrin targeted agent. Gynecologic Oncology. 2013; 128(3):590–595. [PubMed: 23262209]

Hu DE, Kettunen MI, Brindle KM. Monitoring T-lymphocyte trafficking in tumors undergoing immune rejection. Magnetic Resonance in Medicine. 2005; 54(6):1473–1479. [PubMed: 16276491]

Iagaru A, Gambhir SS. Imaging tumor angiogenesis: The road to clinical utility. AJR. American Journal of Roentgenology. 2013; 201(2):W183–W191. [PubMed: 23883233]

Jain RK. Normalizing tumor microenvironment to treat cancer: Bench to bedside to biomarkers. Journal of Clinical Oncology: Official Journal of the American Society of Clinical Oncology. 2013; 31(17):2205–2218. [PubMed: 23669226]

Kakkad SM, Penet MF, Akhbardeh A, Pathak AP, Solaiyappan M, Raman V, et al. Hypoxic tumor environments exhibit disrupted collagen I fibers and low macromolecular transport. PLoS One. 2013; 8(12):e81869. [PubMed: 24349142]

Kakkad SM, Solaiyappan M, Argani P, Sukumar S, Jacobs LK, Leibfritz D, et al. Collagen I fiber density increases in lymph node positive breast cancers: Pilot study. Journal of Biomedical Optics. 2012; 17(11):116017. [PubMed: 23117811]

Kakkad SM, Solaiyappan M, O'Rourke B, Stasinopoulos I, Ackerstaff E, Raman V, et al. Hypoxic tumor microenvironments reduce collagen I fiber density. Neoplasia. 2010; 12(8):608–617. [PubMed: 20689755]

Ko J, Park K, Kim YS, Kim MS, Han JK, Kim K, et al. Tumoral acidic extracellular pH targeting of pH-responsive MPEG-poly(beta-amino ester) block copolymer micelles for cancer therapy. Journal of Controlled Release: Official Journal of the Controlled Release Society. 2007; 123(2): 109–115. [PubMed: 17894942]

Kodibagkar VD, Cui W, Merritt ME, Mason RP. Novel 1H NMR approach to quantitative tissue oximetry using hexamethyldisiloxane. Magnetic Resonance in Medicine. 2006; 55(4):743–748. [PubMed: 16506157]

Lee CP, Payne GS, Oregioni A, Ruddle R, Tan S, Raynaud FI, et al. A phase I study of the nitroimidazole hypoxia marker SR4554 using 19F magnetic resonance spectroscopy. British Journal of Cancer. 2009; 101(11):1860–1868. [PubMed: 19935799]

Li J, Chen K, Liu H, Cheng K, Yang M, Zhang J, et al. Activatable near-infrared fluorescent probe for in vivo imaging of fibroblast activation protein-alpha. Bioconjugate Chemistry. 2012; 23(8):1704–1711. [PubMed: 22812530]

Li Y, Foss CA, Summerfield DD, Doyle JJ, Torok CM, Dietz HC, et al. Targeting collagen strands by photo-triggered triple-helix hybridization. Proceedings of the National Academy of Sciences of the United States of America. 2012; 109(37):14767–14772. [PubMed: 22927373]

Li C, Penet MF, Wildes F, Takagi T, Chen Z, Winnard PT, et al. Nanoplex delivery of siRNA and prodrug enzyme for multimodality image-guided molecular pathway targeted cancer therapy. ACS Nano. 2010; 4(11):6707–6716. [PubMed: 20958072]

Marignol L, Foley R, Southgate TD, Coffey M, Hollywood D, Lawler M. Hypoxia response element-driven cytosine deaminase/5-fluorocytosine gene therapy system: A highly effective approach to overcome the dynamics of tumour hypoxia and enhance the radiosensitivity of prostate cancer cells in vitro. The Journal of Gene Medicine. 2009; 11(2):169–179. [PubMed: 19051213]

Mason RP, Shukla H, Antich PP. In vivo oxygen tension and temperature: Simultaneous determination using 19F NMR spectroscopy of perfluorocarbon. Magnetic Resonance in Medicine. 1993; 29(3): 296–302. [PubMed: 8450738]

Medarova Z, Pham W, Farrar C, Petkova V, Moore A. In vivo imaging of siRNA delivery and silencing in tumors. Nature Medicine. 2007; 13(3):372–377.

Mitsunaga M, Ogawa M, Kosaka N, Rosenblum LT, Choyke PL, Kobayashi H. Cancer cell-selective in vivo near infrared photoimmunotherapy targeting specific membrane molecules. Nature Medicine. 2011; 17(12):1685–1691.

Onnis B, Rapisarda A, Melillo G. Development of HIF-1 inhibitors for cancer therapy. Journal of Cellular and Molecular Medicine. 2009; 13(9A):2780–2786. [PubMed: 19674190]

Pan D, Pramanik M, Senpan A, Allen JS, Zhang H, Wickline SA, et al. Molecular photoacoustic imaging of angiogenesis with integrin-targeted gold nanobeacons. FASEB Journal: Official Publication of the Federation of American Societies for Experimental Biology. 2011; 25(3):875–882. [PubMed: 21097518]

Pascal J, Bearer EL, Wang Z, Koay EJ, Curley SA, Cristini V. Mechanistic patient-specific predictive correlation of tumor drug response with microenvironment and perfusion measurements. Proceedings of the National Academy of Sciences of the United States of America. 2013; 110(35): 14266–14271. [PubMed: 23940372]

Pathak AP, McNutt S, Shah T, Wildes F, Raman V, Bhujwalla ZM. In vivo “MRI phenotyping” reveals changes in extracellular matrix transport and vascularization that mediate VEGF-driven increase in breast cancer metastasis. PLoS One. 2013; 8(5):e63146. [PubMed: 23650550]

Pathak AP, Penet MF, Bhujwalla ZM. MR molecular imaging of tumor vasculature and vascular targets. Advances in Genetics. 2010; 69:1–30. [PubMed: 20807600]

Procissi D, Claus F, Burgman P, Koziorowski J, Chapman JD, Thakur SB, et al. In vivo 19F magnetic resonance spectroscopy and chemical shift imaging of tri-fluoro-nitroimidazole as a potential hypoxia reporter in solid tumors. Clinical Cancer Research. 2007; 13(12):3738–3747. [PubMed: 17575240]

Provent P, Benito M, Hiba B, Farion R, Lopez-Larrubia P, Ballesteros P, et al. Serial in vivo spectroscopic nuclear magnetic resonance imaging of lactate and extracellular pH in rat gliomas shows redistribution of protons away from sites of glycolysis. Cancer Research. 2007; 67(16): 7638–7645. [PubMed: 17699768]

Provenzano PP, Eliceiri KW, Campbell JM, Inman DR, White JG, Keely PJ. Collagen reorganization at the tumor-stromal interface facilitates local invasion. BMC Medicine. 2006; 4(1):38. [PubMed: 17190588]

Quail DF, Joyce JA. Microenvironmental regulation of tumor progression and metastasis. Nature Medicine. 2013; 19(11):1423–1437.

Raman V, Artemov D, Pathak AP, Winnard PT Jr, McNutt S, Yudina A, et al. Characterizing vascular parameters in hypoxic regions: A combined magnetic resonance and optical imaging study of a human prostate cancer model. Cancer Research. 2006; 66(20):9929–9936. [PubMed: 17047055]

Robey IF, Baggett BK, Kirkpatrick ND, Roe DJ, Dosescu J, Sloane BF, et al. Bicarbonate increases tumor pH and inhibits spontaneous metastases. Cancer Research. 2009; 69(6):2260–2268. [PubMed: 19276390]

Ross RW, Zietman AL, Xie W, Coen JJ, Dahl DM, Shipley WU, et al. Lymphotropic nanoparticle-enhanced magnetic resonance imaging (LNMRI) identifies occult lymph node metastases in prostate cancer patients prior to salvage radiation therapy. Clinical Imaging. 2009; 33(4):301–305. [PubMed: 19559353]

Schmieder AH, Caruthers SD, Zhang H, Williams TA, Robertson JD, Wickline SA, et al. Three-dimensional MR mapping of angiogenesis with alpha5beta1(alpha nu beta3)-targeted theranostic nanoparticles in the MDA-MB-435 xenograft mouse model. FASEB Journal: Official Publication of the Federation of American Societies for Experimental Biology. 2008; 22(12):4179–4189. [PubMed: 18697838]

Schmieder AH, Winter PM, Williams TA, Allen JS, Hu G, Zhang H, et al. Molecular MR imaging of neovascular progression in the Vx2 tumor with alphavbeta3-targeted paramagnetic nanoparticles. Radiology. 2013; 268(2):470–480. [PubMed: 23771914]

Seenu V, Pavan Kumar MN, Sharma U, Gupta SD, Mehta SN, Jagannathan NR. Potential of magnetic resonance spectroscopy to detect metastasis in axillary lymph nodes in breast cancer. Magnetic Resonance Imaging. 2005; 23(10):1005–1010. [PubMed: 16376185]

Semenza GL. Defining the role of hypoxia-inducible factor 1 in cancer biology and therapeutics. Oncogene. 2010; 29(5):625–634. [PubMed: 19946328]

Servagi-Vernat S, Differding S, Hanin FX, Labar D, Bol A, Lee JA, et al. A prospective clinical study of F-FAZA PET-CT hypoxia imaging in head and neck squamous cell carcinoma before and during radiation therapy. European Journal of Nuclear Medicine and Molecular Imaging. 2014; 41(8):1544–1552. [PubMed: 24570097]

Shih YY, Hsu YH, Duong TQ, Lin SS, Chow KP, Chang C. Longitudinal study of tumor-associated macrophages during tumor expansion using MRI. NMR in Biomedicine. 2011; 24(10):1353–1360. [PubMed: 22223366]

Spence AM, Muzi M, Swanson KR, O'Sullivan F, Rockhill JK, Rajendran JG, et al. Regional hypoxia in glioblastoma multiforme quantified with [18F]fluoromisonidazole positron emission tomography before radiotherapy: Correlation with time to progression and survival. Clinical Cancer Research: An Official Journal of the American Association for Cancer Research. 2008; 14(9):2623–2630. [PubMed: 18451225]

Stasinopoulos I, Penet MF, Chen Z, Kakkad S, Glunde K, Bhujwalla ZM. Exploiting the tumor microenvironment for theranostic imaging. NMR in Biomedicine. 2011; 24(6):636–647. [PubMed: 21793072]

Thomlinson RH, Gray LH. The histological structure of some human lung cancers and the possible implications for radiotherapy. British Journal of Cancer. 1955; 9(4):539–549. [PubMed: 13304213]

Vahrmeijer AL, Hutteman M, van der Vorst JR, van de Velde CJ, Frangioni JV. Image-guided cancer surgery using near-infrared fluorescence. Nature Reviews Clinical Oncology. 2013; 10(9):507–518.

van Dam GM, Themelis G, Crane LM, Harlaar NJ, Pleijhuis RG, Kelder W, et al. Intraoperative tumor-specific fluorescence imaging in ovarian cancer by folate receptor-alpha targeting: First in-human results. Nature Medicine. 2011; 17(10):1315–1319.

van Sluis R, Bhujwalla ZM, Raghunand N, Ballesteros P, Alvarez J, Cerdan S, et al. In vivo imaging of extracellular pH using ^{1}H MRSI. Magnetic Resonance in Medicine. 1999; 41(4):743–750. [PubMed: 10332850]

Vandsburger MH, Radoul M, Addadi Y, Mpofu S, Cohen B, Eilam R, et al. Ovarian carcinoma: Quantitative biexponential MR imaging relaxometry reveals the dynamic recruitment of ferritin-

expressing fibroblasts to the angiogenic rim of tumors. Radiology. 2013; 268(3):790–801. [PubMed: 23801774]

Wang Z, Yu Y, Ma J, Zhang H, Wang X, Wang J, et al. LyP-1 modification to enhance delivery of artemisinin or fluorescent probe loaded polymeric micelles to highly metastatic tumor and its lymphatics. Molecular Pharmaceutics. 2012; 9(9):2646–2657. [PubMed: 22853186]

Wang L, Zhu X, Xie C, Ding N, Weng X, Lu W, et al. Imaging acidosis in tumors using a pH-activated near-infrared fluorescence probe. Chemical Communications. 2012; 48(95):11677–11679. [PubMed: 23095940]

Weidle UH, Tiefenthaler G, Georges G. Proteases as activators for cytotoxic prodrugs in antitumor therapy. Cancer Genomics & Proteomics. 2014; 11(2):67–79. [PubMed: 24709544]

Winter PM, Schmieder AH, Caruthers SD, Keene JL, Zhang H, Wickline SA, et al. Minute dosages of alpha(nu)beta3-targeted fumagillin nanoparticles impair Vx-2 tumor angiogenesis and development in rabbits. FASEB Journal: Official Publication of the Federation of American Societies for Experimental Biology. 2008; 22(8):2758–2767. [PubMed: 18362202]

Yang H, Zou LG, Zhang S, Gong MF, Zhang D, Qi YY, et al. Feasibility of MR imaging in evaluating breast cancer lymphangiogenesis using Polyethylene glycol-GoldMag nanoparticles. Clinical Radiology. 2013; 68(12):1233–1240. [PubMed: 23969152]

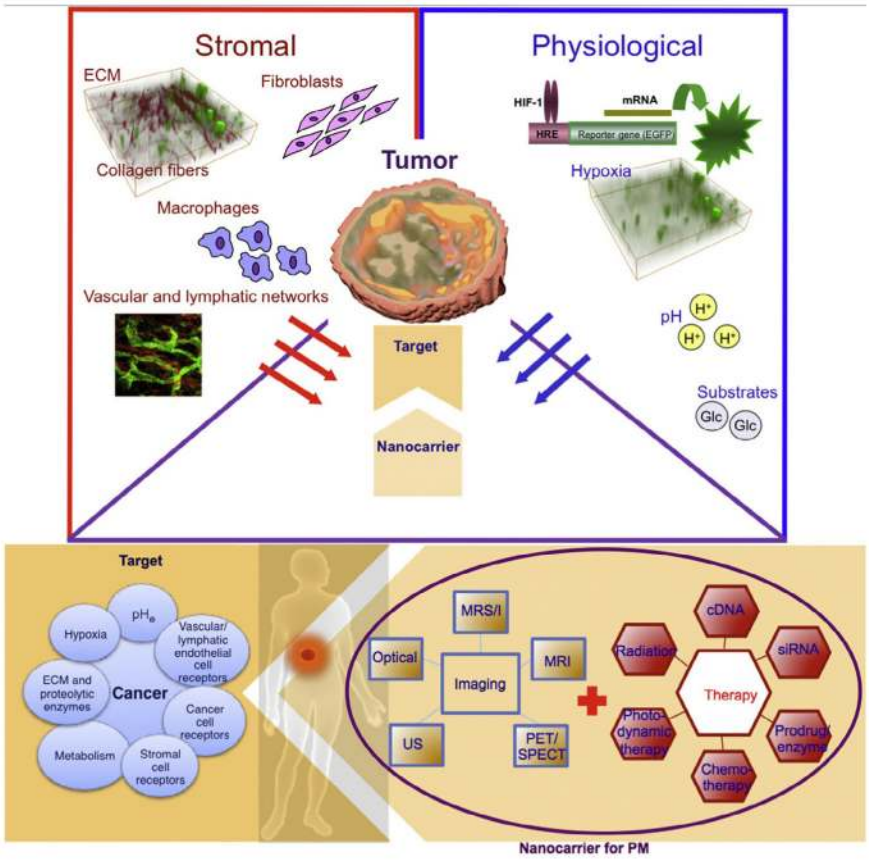

Figure 7.1.

Schematic overview of precision medicine strategies exploiting the tumor microenvironment. *Adapted from* Stasinopoulos et al. (2011).

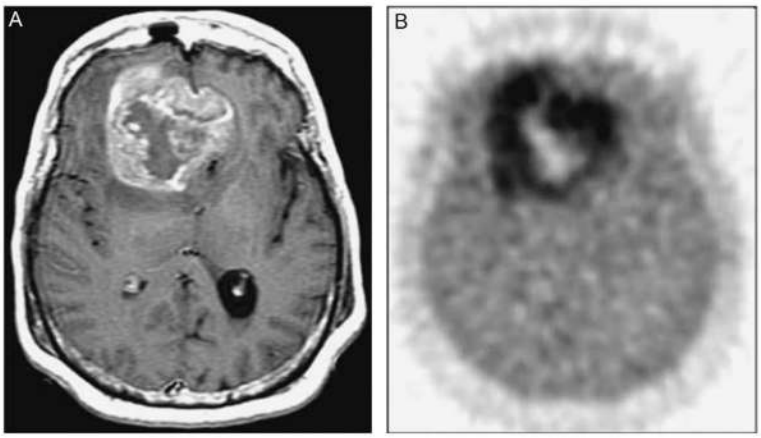

Figure 7.2.

(A and B) A 55-year-old woman with a bifrontal GBM imaged after a biopsy. (A) MRI T_1-Gadolinium showing a large contrast-enhancing irregular ring-shaped tumor with a necrotic center. (B) FMISO image through the same plane. The hypoxic volume was 129 cm^3, and the maximum tissue to blood concentration was 3.0. *Adapted with permission from* Spence et al. (2008).

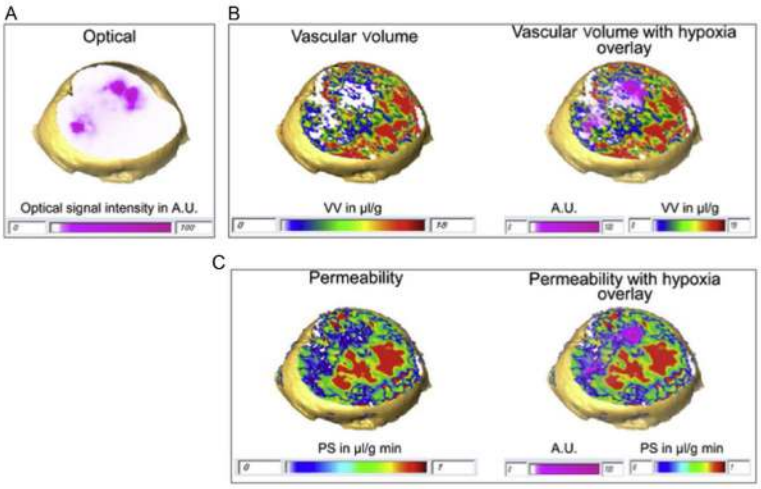

Figure 7.3.

Three-dimensional reconstruction of (A) optical image with hypoxic regions displayed in gray within the tumor, (B) corresponding display of vascular volume (left), and overlay of hypoxia mask on vascular volume (right), (C) corresponding display of permeability surface area product (left) and overlay of hypoxia mask on permeability surface area product (right) in a breast cancer xenograft. To visualize the hypoxic mask, all voxels with signal intensity higher than 10% of the maximum fluorescence signal intensity in each optical image were included. This was done to avoid using a hard threshold and to exclude any background signal due to autofluorescence. *Adapted with permission from* Kakkad et al. (2013).

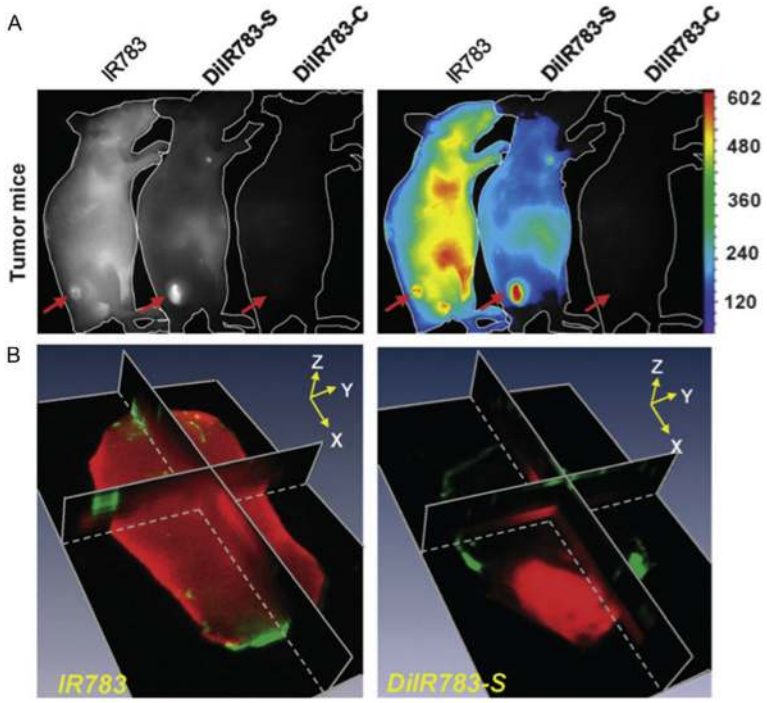

Figure 7.4.

(A) Representative NIR fluorescence and color-coded fluorescence images of MDA-MB-465 tumor-bearing mice at 24 h postinjection. Arrows point to the tumor. (B) 3D reconstructed fluorescence images of tumors at 24 h postinjection. The NIR fluorescence is displayed in red, and the vasculature stained by DiO is displayed in green. *Adapted with permission from* Wang, Zhu, et al. (2012).

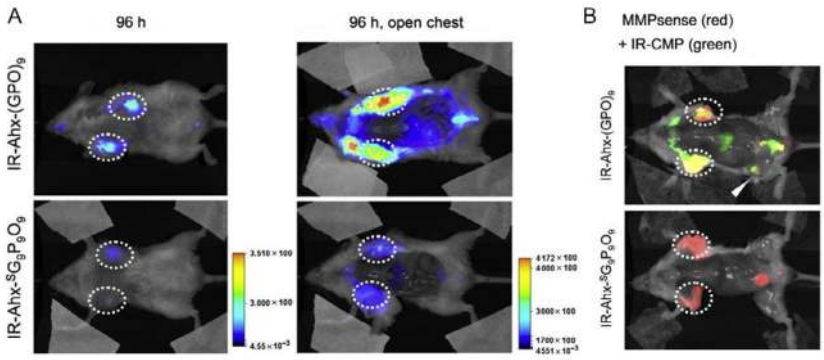

Figure 7.5.

In vivo targeting of tumors by CMP hybridization with MMP-digested collagens. (A) *In vivo* NIR fluorescent images of mice bearing PC-3 prostate tumors on the right and left flank (circled) administered with 3.7 nmol of UV-activated IR-Ahx-NB $(GPO)_9$ or sequence-scrambled control peptide. Ventral views of both mice at 96 h post-injection, and after midline surgical laparotomy indicate tumor specific and stable accumulation of the IR-Ahx-$(GPO)_9$ peptide. (B) NIR fluorescent images of another pair of mice bearing PC-3 tumors at the same location at 102 h after IR-CMP injection and 24 h after MMPSense680 injection, showing colocalization (in yellow) of MMP activity (red) and CMP binding (green) in the tumors (circled) and knee joint (arrowhead). *Adapted with permission from* Li, Foss, et al. (2012).

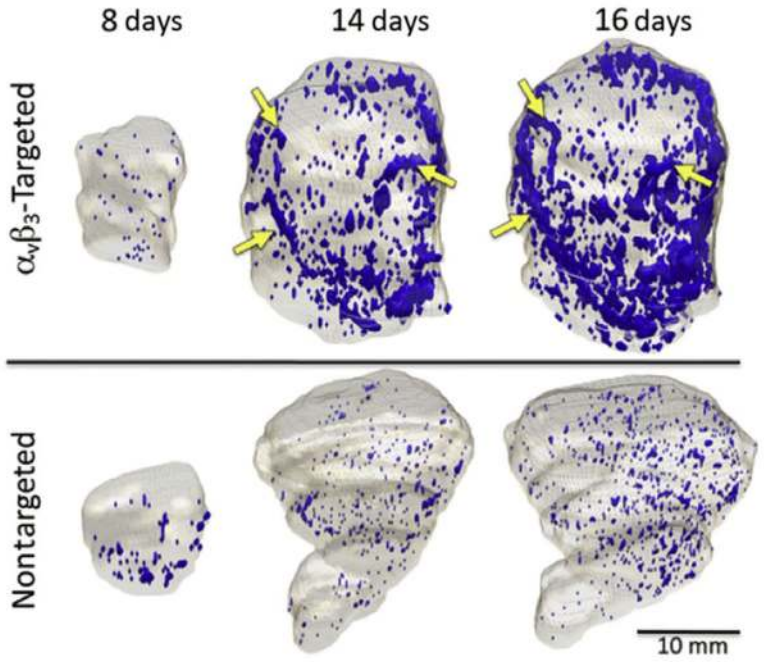

Figure 7.6.

Neovascular maps showing contrast-enhanced voxels over time. Increase in significantly enhanced tumor voxels is clearly apparent on 3D reconstructions of MR signal enhancement derived from paramagnetic nanoparticles. Tumor volume is outlined in gray, and contrast-enhanced pixels are shown in blue. Maps illustrate that MRI detection of neovessels markedly increased between days 8 and 14, with continued spatial progression noted on day 16. Arrows indicate examples of consistent enhancement patterns over time. The tumor of the rabbit that received nontargeted paramagnetic nanoparticles shows little enhancement despite continued tumor growth and progression of neovessels. *Adapted with permission from* Schmieder et al. (2013).

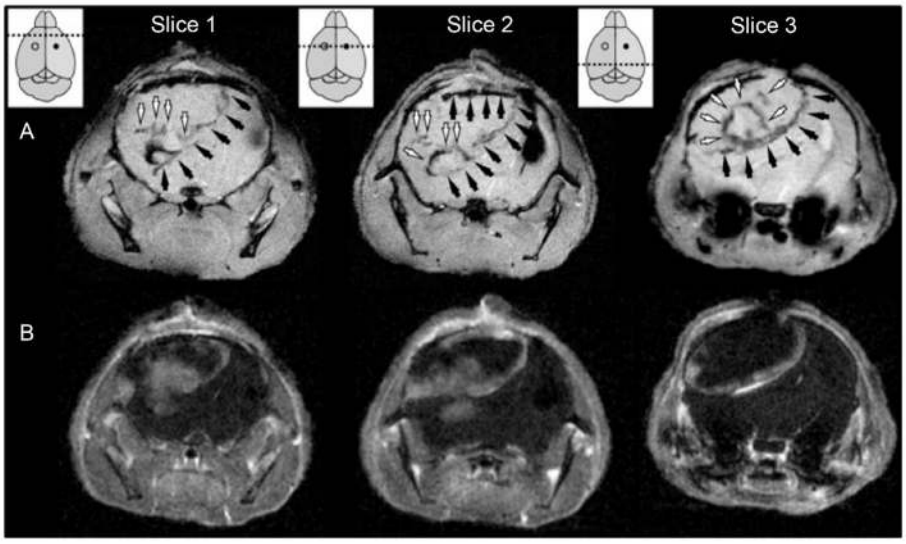

Figure 7.7.

Tropism of MPIO-labeled stem cells toward areas of high permeability at the edge of and inside U87vIII tumors following contralateral injections. (A) Axial T_2*-weighted images of a U87vIII tumor-bearing mouse 7 days after contralateral injection of MPIO-labeled human mesenchymal stem cells and (B) corresponding contrast-enhanced-MR images, confirming the colocalization of MPIO-induced areas of hyposignal with the edges of the postgadolinium-enhancing tumors. The MPIO-labeled stem cells injection sites are shown as empty circles, the tumor injection sites as filled circles. The dotted lines show the localization of the displayed imaging slices. MPIO-labeled stem cells localized at the edges of the tumors in areas of high permeability (black arrows) and inside the tumor masses (white arrows). *Adapted with permission from* Chaumeil et al. (2012).